Quantifying strength of chaos in the population firing rate of neurons

Takashi Kanamaru

Department of Mechanical Science and Engineering,
School of Advanced Engineering, Kogakuin University,
Hachioji-city, Tokyo 192-0015, Japan

Abstract

In this study, I considered quantifying the strength of chaos in the population firing rate of a pulse-coupled neural network. In particular, I considered the dynamics where the population firing rate is chaotic and the firing of each neuron is stochastic. I calculated a time histogram of firings to show the variation in the population firing rate over time. To smooth this histogram, I used Bayesian adaptive regression splines and a gaussian filter. The nonlinear prediction method, based on reconstruction, was applied to a sequence of interpeak intervals in the smoothed time histogram of firings. I propose the use of the sum of nonlinearity as a quantifier of the strength of chaos. When applying this method to the firings of a pulse-coupled neural network, the sum of nonlinearity was seen to satisfy three properties for quantifying the strength of chaos. First, it can be calculated from spiking data alone. Second, it takes large values when applied to firings that are confirmed, theoretically or numerically, to be chaotic. Third, it reflects the strength of chaos of the original dynamics.

1 Introduction

It is well known that the firing pattern of cortical neurons is highly irregular, and its role in information processing has been discussed previously (Softky & Koch, 1993). There are several sources of fluctuations that may cause such irregular firing, such as random fluctuations of ion channels between open and closed states (Conti et al., 1975), and unreliable synaptic transmission, caused by a stochastic release of chemical transmitters (Hessler et al., 1993). Since such stochasticity is caused by thermal fluctuations, it would be difficult to eliminate. Yet when the amounts of excitatory and inhibitory synaptic inputs to a neuron are balanced, highly irregular firing is observed (Shadlen & Newsome, 1994). If such synaptic inputs cause an irregular firing pattern in cortical neurons, seemingly noisy firings may play important roles in information processing within the brain.

Findings related to such irregular firing have been reported in both theoretical and physiological studies. For example, it has previously been reported that a model of a network with balanced excitatory and inhibitory activity exhibits chaotic dynamics (Vreeswijk & Sompolinsky, 1996). In the rat barrel cortex, sensitive dependence on perturbation of inputs has been observed, in vivo (London et al., 2010). Although the mechanism that causes this phenomenon remains unknown, some authors have related it to the concept of "stable chaos" that is characterized by the negative largest Lyapunov exponent (Politi & Torcini, 2010; Monteforte & Wolf, 2012; Angulo-Garcia & Torcini, 2014). It is also possible to relate this phenomenon to the conventional chaotic dynamics that is characterized by the positive largest Lyapunov exponent (Ott, 2002). In this study, I focus on conventional chaotic dynamics characterized by the positive largest Lyapunov exponent in the brain.

If chaos exists in the brain, it is important to develop a method by which it can be quantified experimentally. A nonlinear prediction method, based on reconstruction, is often used to examine whether chaos exists in the spike sequence of a neuron (Theiler et al., 1992; Sauer, 1994; Hegger, Kantz, & Schreiber, 1999; Schreiber & Schmitz, 2000). However, this method requires knowledge of the precise timing of each spike, and it is unreliable in the presence of spikes caused by noise (Kanamaru & Sekine, 2005). Therefore, to decrease the contribution of pulses caused by noise, a method by which the strength of chaos in the population firing rate of neurons can be quantified is required. For this purpose, several conditions are prerequisite. First, this method should quantify the strength of chaos from spiking data only, and it should not require detailed information about the system. If stochastic differential equations that govern the system are known, it is possible to estimate the largest Lyapunov exponent (Angulo-Garcia & Torcini, 2015). However, I will not take this approach, as I seek to apply the proposed method to experimental data. Second, the strength of chaos obtained by the proposed method should take large values when applied to firings that are confirmed, either theoretically or numerically, to be chaotic. Third, the strength of chaos obtained by the proposed method should reflect the strength of chaos of the original dynamics. To satisfy these conditions, I required a theoretical model that exhibits chaotic firing, whose largest Lyapunov exponent can be numerically calculated. More-

over, it should be possible to control the strength of chaos of this model by regulating its parameters.

For this purpose, I used a pulse-coupled neural network proposed by Kanamaru & Aihara (2008). This network exhibits various synchronizations, including chaotic synchronizations. Typical chaotic synchronization is characterized by chaotic oscillations of the ensemble-averaged firing rate, with a large amplitude. This synchronization has the positive largest Lyapunov exponent in the limit of a large number of neurons. Typically, in such chaotic synchronization, the firing of each neuron is stochastic, and its firing rate is close to the main frequency of the ensemble-averaged firing rate. Moreover, this network also exhibits stochastic synchronization of chaos, where the ensemble-averaged dynamics in neuronal assemblies exhibit chaotic oscillations with a small amplitude and each neuron has a low firing rate. I used such strong and weak chaotic synchronizations as two examples in which to apply my method for quantifying the strength of chaos.

Stochastic synchrony (Tiesinga & José, 2000; Brunel & Hansel, 2006), where the ensemble-averaged dynamics in neuronal assemblies exhibit oscillations, although with a low firing rate for each neuron, is often observed in the visual cortex (Gray & Singer, 1989), the hippocampus (Buzsáki et al., 1992; Csicsvari et al., 1998; Fisahn et al., 1998; Whittington et al., 2000), and the cerebellar nucleo-olivary pathway (Lang et al., 1996). Stochastic synchrony has been found in modeling studies based on experimental data (Traub et al., 1989), as well as in theoretical modeling studies (Brunel, 2000; Brunel & Hansel, 2006; Kanamaru & Sekine, 2004, 2006). Its relationship with information processing has attracted much attention. Although stochastic synchrony is typically composed of periodic oscillations, in this study, I considered stochastic synchrony with chaotic oscillations (Kanamaru & Aihara, 2008). One of the mechanisms underlying stochastic synchrony might be oscillations with small amplitudes in the ensemble-averaged dynamics of the network. If one considers a situation where dynamics averaged over an assembly of neurons exhibit oscillation, then this oscillation becomes a feedback input into the network. If the amplitude of this feedback input is sub-threshold for each neuron, then the firing of each neuron becomes stochastic, and stochastic synchrony occurs (Kanamaru & Sekine, 2004, 2006). This mechanism is similar to that underlying stochastic resonance (Gammaitoni et al., 1998).

My method for quantifying the strength of chaos is based on the nonlinear prediction method (Theiler et al., 1992; Sauer, 1994). However, because the firings of each neuron are stochastic in my model, the nonlinear prediction method should be applied to the population firing rate of neurons, rather than to the spike sequence of each neuron. The time series of the population firing rate is noisy, and therefore appropriate smoothing methods are required. I used Bayesian adaptive regression splines (BARS) for smoothing (Dimatteo et al., 2001; Wallstrom et al., 2008). BARS approximate a time series of the population firing rate as a linear combination of cubic splines, where their number and temporal positions vary. The data approximated with BARS follow sudden

changes in the population firing rate (Kass et al., 2005; Wallstrom et al., 2008). For comparison, I also used smoothing by means of a gaussian filter. Using the smoothed population firing rate, I could calculate a sequence of interpeak intervals (IPIs), and the nonlinear prediction method could be applied to this sequence.

The remainder of this paper is organized as follows: In section 2, I define a network comprising excitatory and inhibitory neurons and then introduce two classes of chaotic firing. Firing where the population firing rate is chaotic and the firing rate of each neuron is stochastic is called the rate synchrony of chaos (RSC). Firing where the population firing rate is chaotic and the firing rate of each neuron is much lower than that of the RSC is called stochastic synchrony of chaos (SSC). In section 3, I define the time histogram of firings to show variations in the population firing rate over time. I also employ BARS and a gaussian filter as methods to smooth the time histogram of firings. In section 4, I describe quantification of the strength of chaos in the smoothed histogram of firings, and I examine how chaos is lost when the number of neurons in the network and the number of observed neurons decrease. The results are discussed, and I present my conclusions in section 5.

2 Model

I consider a pulse-coupled neural network defined in Kanamaru & Aihara (2008), comprising N excitatory neurons and N inhibitory neurons with the internal states $\theta_E^{(i)}$ and $\theta_I^{(i)}$ ($i = 1, 2, \cdots, N$) governed by the following equations:

$$\tau_E \dot{\theta}_E^{(i)} = (1 - \cos\theta_E^{(i)}) + (1 + \cos\theta_E^{(i)})$$
$$\times (r_E + \eta_E^{(i)}(t) + g_{EE}I_E(t) - g_{EI}I_I(t)) \quad (2.1)$$

$$\tau_I \dot{\theta}_I^{(i)} = (1 - \cos\theta_I^{(i)}) + (1 + \cos\theta_I^{(i)})$$
$$\times (r_I + \eta_I^{(i)}(t) + g_{IE}I_E(t) - g_{II}I_I(t)$$
$$+ g_{gap}I_{gap}^{(i)}(t)), \quad (2.2)$$

$$I_X(t) = \frac{1}{2N}\sum_{j=1}^{N}\sum_{k}\frac{1}{\kappa_X}\exp\left(-\frac{t - t_k^{(j)}}{\kappa_X}\right), \quad (2.3)$$

$$I_{gap}^{(i)}(t) = \frac{1}{N}\sum_{j=1}^{N}\sin\left(\theta_I^{(j)}(t) - \theta_I^{(i)}(t)\right), \quad (2.4)$$

$$\langle\eta_X^{(i)}(t)\eta_Y^{(j)}(t')\rangle = D\delta_{XY}\delta_{ij}\delta(t - t'), \quad (2.5)$$

where r_E and r_I are parameters of the neurons that determine whether the equilibrium of each neuron is stable. I use $r_E = r_I = -0.025$ to ensure that each neuron has a stable equilibrium. $X = E$ or I denotes the excitatory or inhibitory ensemble, respectively, while $t_k^{(j)}$ is the kth firing time of the jth neuron in the ensemble X, and firing time is defined as the time when $\theta_X^{(j)}$ exceeds π, after which $\theta_X^{(j)}$ resets to $-\pi$. Neurons communicate with each other via postsynaptic potentials, the waveforms of which are exponential functions, as shown in equation 2.3. $\eta_X^{(i)}(t)$ represents
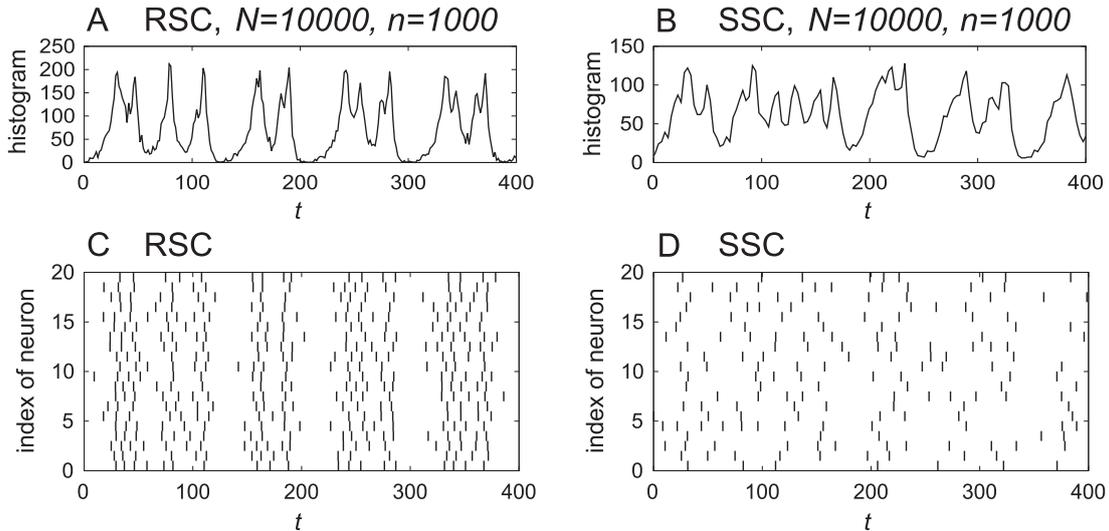
Figure 1: Firing of excitatory neurons in the network with $N = 10,000$. (A, B) Time histogram of firings, calculated based on observation of the firing of 1000 neurons. (C, D) Raster plot based on the firing of 20 neurons. (A, C) Rate synchrony of chaos (RSC), observed with $g_{ext} = 3.9$ and $D = 0.006$. (B, D) Stochastic synchrony of chaos (SSC), observed with $g_{ext} = 4.4$ and $D = 0.0045$.

gaussian white noise added to the ith neuron in the ensemble X. The network comprises theta neurons (Ermentrout, 1996; Izhikevich, 1999, 2000), which yield spikes when sufficiently large inputs are injected. For simplicity, I set the parameters as $g_{EE} = g_{II} \equiv g_{int}, g_{EI} = g_{IE} \equiv g_{ext}, g_{int} = 5$, $g_{gap} = 0.15, \tau_E = 1, \tau_I = 0.5, \kappa_E = 1$, and $\kappa_I = 5$. g_{int} and g_{ext} are the internal connection strength in an ensemble and the external connection strength between excitatory and inhibitory ensembles, respectively. I use these parameter values because, under such conditions, the network yields chaos with various firing rates in the limits of a large number of neurons (Kanamaru & Aihara, 2008). Because the purpose of this study is to quantify the strength of chaos in the population firing rates of neurons, it is desirable to know in advance whether the examined dynamics are indeed chaotic.

Unlike the network used in Kanamaru (2006), the network defined by equations 2.1 and 2.2 incorporates connections with gap junctions amongst inhibitory neurons, according to previous experimental studies that showed that inhibitory neurons in many areas of the brain, such as the cortex and the hippocampus (Galarreta & Hestrin, 2001) are rich in electrical synapses. Typically, the gap junctions facilitate the synchronization in the system, and they are often modeled by diffusive couplings that are proportional to the difference in the voltages (Munro & Börgers, 2010). For networks of phase models, the diffusive couplings are represented by sinusoidal terms of the phase difference (Kuramoto, 1984). I used a network including gap junctions, as it exhibits rich chaotic dynamics, with various firing rates. Without gap junctions, chaotic firings with only high firing rates are observed; however, by introducing gap junctions, chaotic firings with low firing rates are also observed, as I show below.

Note that for simplicity, the number of neurons in the excitatory ensemble and the inhibitory ensemble are set to the

identical value N in this model. Even when each ensemble includes a different number of neurons, the dynamics in the limit of a large number of neurons will remain unchanged, because the connections defined by equations 2.3 and 2.4 are divided by the number of neurons.

As for the outputs of the network, I observed the sequences of the firing times for n excitatory neurons, selected randomly from N excitatory neurons.

The typical chaotic firings considered in this study are shown in Figure 1. The firings of the excitatory neurons in the network with $N = 10,000$ for $g_{ext} = 3.9$ and $D = 0.006$ are shown in Figures 1A and 1C. Figure 1A shows a histogram of the firings, as defined in the next section, which represents the variation in the population firing rate over time, as calculated from observation of the firing of 1000 excitatory neurons. The value of the bin size Δ in the time histogram of firings is set as $\Delta = 1.5$, based on the method proposed by Shimazaki & Shinomoto (2007), as explained in the next section. Figure 1C shows a raster plot based on the firing of 20 randomly selected excitatory neurons. In Figures 1A and 1C, it can be seen that each neuron fires once or twice, around the peak of the time histogram of firings, and their timings fluctuate around the precise position of each peak.

In the limit of $N \to \infty$, the ensemble-averaged dynamics governed by equations 2.1 and 2.2 can be analyzed using the Fokker-Planck equation defined in Appendix A, and it can be confirmed numerically that the population firing rate shown in Figure 1A is chaotic (Kanamaru & Aihara, 2008). In this study, I refer to the dynamics, where the population firing rate is chaotic and the firing of each neuron is stochastic, as the RSC.

The firings for $g_{ext} = 4.4$ and $D = 0.0045$ are shown in Figures 1B and 1D. Figure 1B shows a time histogram
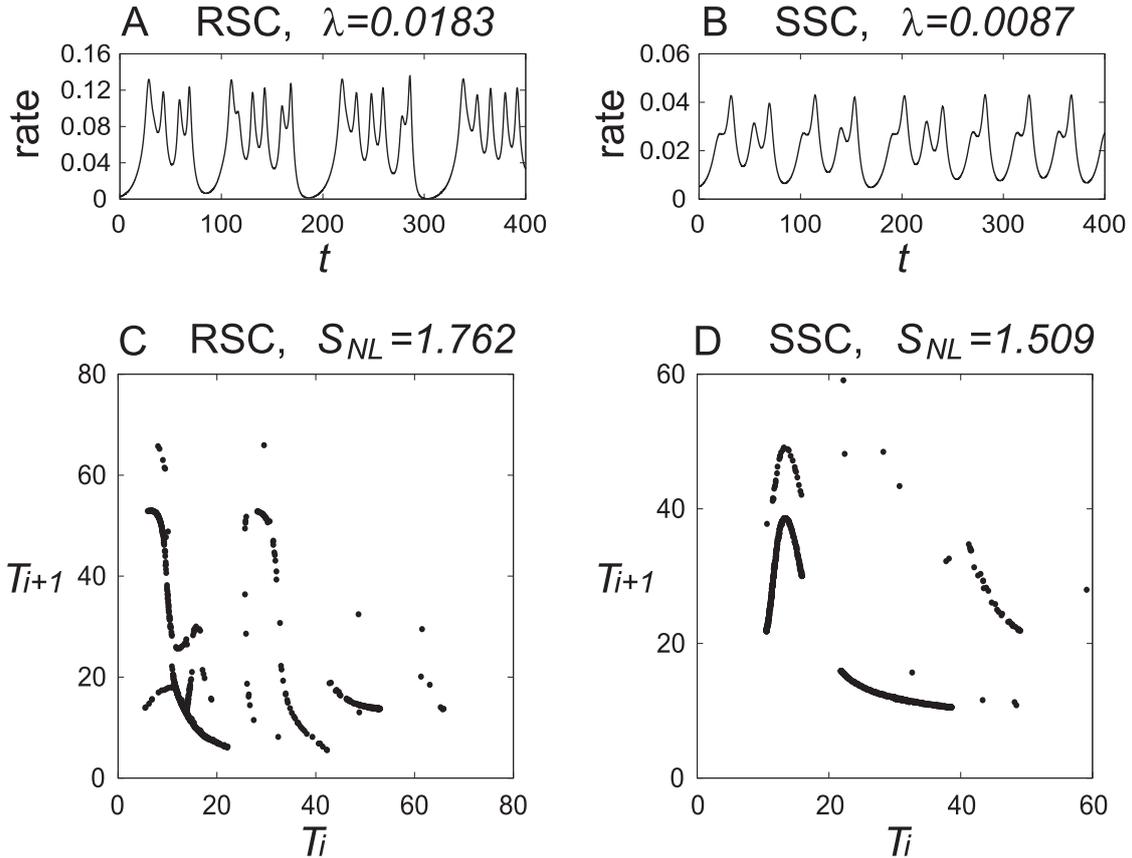
3

Figure 2: Dynamics in the limit of $N \to \infty$. (A, B) Instantaneous firing rates in the network. (C, D) Return plots for the interpeak interval T_i. (A, C) RSC corresponding to Figures 1A and 1C. (B, D) SSC corresponding to Figures 1B and 1D.

of firings with $\Delta = 3.0$, calculated based on the observed firing of 1000 excitatory neurons. Figure 1D shows a raster plot based on the firing of 20 randomly selected excitatory neurons. It can be seen that the probability of firing around the peak of the population firing rate is low, which is a typical property of stochastic synchrony (Tiesinga & José, 2000; Brunel & Hansel, 2006). The firings shown in Figures 1B and 1D, are also confirmed as being chaotic in the limit of $N \to \infty$; therefore, I refer to the firings shown in Figures 1B and 1D as SSC, which is a special case of RSC (Kanamaru & Aihara, 2008).

In the previous work, I characterized SSC by the difference between the main frequency of the ensemble-averaged dynamics and that of the firing of each neuron (Kanamaru & Aihara, 2008). The main frequency was defined as the frequency at the position of broad peak of the power spectrum of the ensemble-averaged firing rate in Kanamaru & Aihara (2008). The main frequency f_{all} of the ensemble-averaged dynamics of the data in Figure 1B is $f_{all} = 0.046$, and the mean frequency of the firing of each neuron in Figure 1D is $f_1 = 0.017$. Because f_1 is much smaller than f_{all}, the dynamics in Figures 1B and 1D were called SSC in Kanamaru & Aihara (2008). In the case of Figure 1A and 1C, the frequencies are calculated to be $f_{all} = 0.038$ and $f_1 = 0.041$. In this case, f_{all} and f_1 take similar values; therefore, the

dynamics in Figures 1A and 1C could be distinguished from SSC in Kanamaru & Aihara (2008), and I term them RSC in this study. I use RSC and SSC as examples to quantify the strength of chaos. Note that the boundary between SSC and RSC is determined based on the ratio of f_1 to f_{all}, and its value can arbitrarily be chosen. The main concern of Kanamaru & Aihara (2008) was the dynamics of a pulse-coupled neural network, and not its statistical properties. Moreover, the boundary between SSC and RSC does not affect the result of this study. Therefore, I will not discuss this boundary further.

3 Smoothing the time histogram of firings and calculating the IPI

In this section, I quantify the strength of chaos in firings by a network with a finite number of neurons, as shown in Figure 1.

First, for comparison, I discuss the dynamics of RSC and SSC in the limit of $N \to \infty$, using the Fokker-Planck equation defined in Appendix A (Kanamaru & Aihara, 2008). The instantaneous firing rates defined by equations A.11 and A.12 calculated from the Fokker-Planck equation are shown in Figures 2A and 2B, which correspond to the time his-
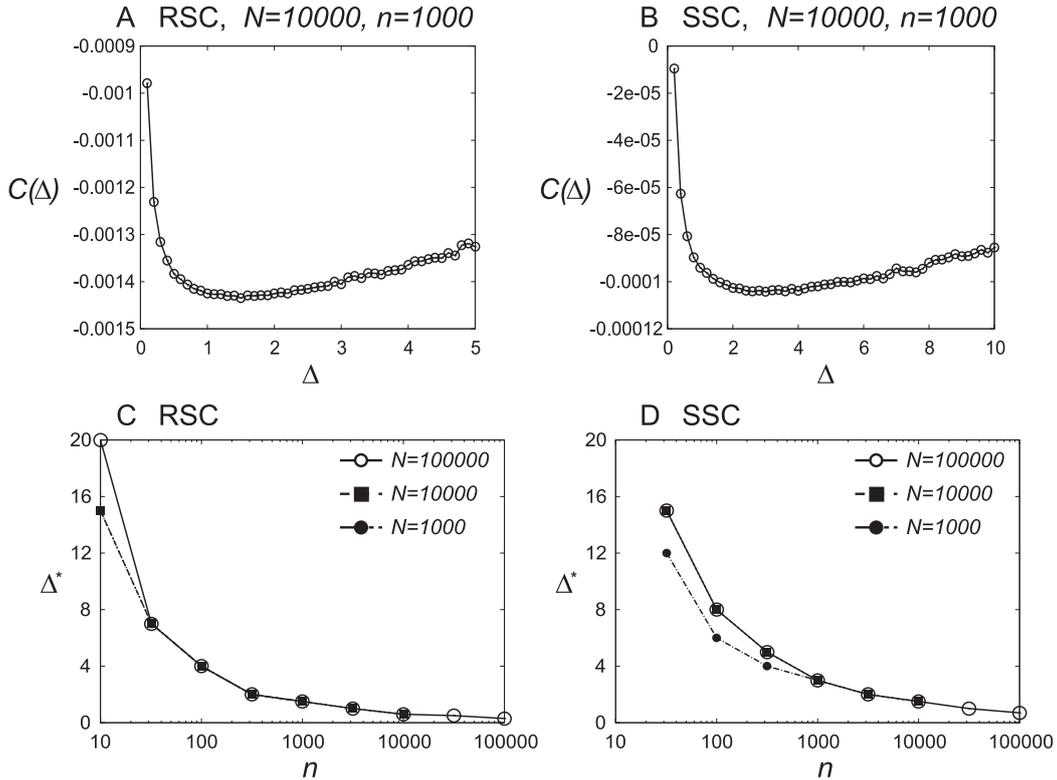
4

Figure 3: (A, B) Cost function $C(\Delta)$ for (A) RSC and (B) SSC. Dependence of the optimal Δ^* on the observed number n of neurons with various N for (C) RSC and (D) SSC.

tograms of firings in Figures 1A and 1B, respectively, divided by $n\Delta$ in the limit of $N = n \to \infty$ and $\Delta \to 0$.

In the limit of $N \to \infty$, the largest Lyapunov exponents can be numerically calculated to be $\lambda = 0.0183$ and 0.0087 for RSC and SSC, respectively. For the numerical calculation of the largest Lyapunov exponents, I used a standard technique (Ott, 2002; Kanamaru, 2006); namely, I calculated the expansion rate of two nearby trajectories, each of which follows a set of ordinary differential equations of the spatial Fourier coefficients defined by equations A.13, A.16, and A.17.

The instantaneous firing rate is a smooth function of time t, and thus it is easy to obtain the ith peak time t_i at which the instantaneous firing rate takes the local maxima. Using the IPI $T_i \equiv t_{i+1} - t_i$, return plots in the (T_i, T_{i+1}) plane are shown in Figures 2C and 2D. In Figure 2C, two decreasing sections for $0 < T_i < 23$ and $28 < T_i < 43$ are observed, which are similar to the Bernoulli shift (Ott, 2002). In Figure 2D, parabolic structures are observed, which are similar to the logistic map (Ott, 2002). Both structures are typical of low-dimensional chaos. The sum of nonlinearity S_{NL} defined in section 4 is also shown in Figures 2C and 2D, which takes large positive values when the dynamics are chaotic. Note that the largest Lyapunov exponent λ, shown in Figures 2A and 2B, relates to the expansion rate of two nearby trajectories of continuous-time dynamics (Ott, 2002). On the other hand, S_{NL}, shown in Figures 2C and 2D, relates to discrete-time dynamics of T_i. Therefore, there is no direct relationship between λ and S_{NL}. The meaning of the values of S_{NL} will be discussed in section 4, after defining S_{NL}.

In order to find similar structures in a network with finite N, I calculated the time histogram based on the observed firings of n excitatory neurons. According to Shimazaki & Shinomoto (2007), I divided the time axis into L bins, with width Δ, and counted the number k_i of firings in the ith bin. The width Δ is determined as the value Δ^* that minimizes the cost function.

$$C(\Delta) \equiv \frac{2\bar{k} - v}{(n\Delta)^2}, \qquad (3.1)$$

$$\bar{k} \equiv \frac{1}{L}\sum_{i=1}^{L} k_i, \qquad (3.2)$$

$$v \equiv \frac{1}{L}\sum_{i=1}^{L}(k_i - \bar{k})^2. \qquad (3.3)$$

The cost functions $C(\Delta)$ for the data used in Figures 1A and 1B are shown in Figures 3A and 3B, respectively, and, as values of Δ that minimize $C(\Delta)$, $\Delta^* = 1.5$ and 3.0 are chosen. Δ^* depends on N, n, and the parameters of the network. In Figures 3C and 3D, the dependence of Δ^* on the number n of observed neurons with various N is shown for RSC and SSC, respectively. It is observed that Δ^* becomes large as n decreases because the number of firings is small. Moreover, small Δ^* for large n could be caused by the large

5

variability of firings among neurons. It is also observed that the dependence of Δ^* on N is marginal.
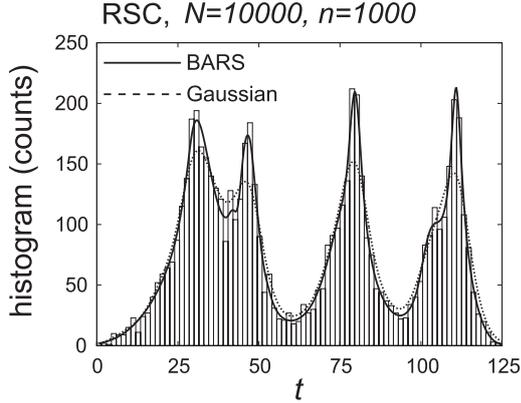

Figure 4: Time histogram of firings with $\Delta = \Delta^* = 1.5$ and smoothed time histograms of firings for RSC. The solid and broken lines show the time histograms of firings smoothed with BARS and with a gaussian filter, respectively. The bandwidth Δ_g of the gaussian filter was set to the value $\Delta_g^* = 3.0$, which maximized the sum of nonlinearity, as defined in section 4.

The time histogram of firings for RSC with $\Delta = \Delta^* = 1.5$ is shown in Figure 4, which is identical to that in Figure 1A in the range of $0 \leq t \leq 125$. I defined the peak time of the time histogram of firings as the time at which this histogram takes local maxima. Therefore, when the shape of the time histogram of firings is noisy, many undesirable peak times will be detected due to noise, and smoothing of the time histogram is required. I used BARS (Dimatteo et al., 2001) and a gaussian filter (Kass et al., 2005) as smoothing methods.

BARS approximate the time histogram of firings as a linear combination of cubic splines, with a variable number of knots and temporal positions. First, the center position of the ith bin of the time histogram in $[0, T]$ is defined as t_i ($i = 1, 2, \cdots, L$), and the number of firings in the ith bin is k_i, as defined above. It is assumed that k_i obeys a Poisson distribution with mean μ_i, that is,

$$P(k_i) = e^{-\mu_i} \frac{\mu_i^{k_i}}{k_i!}. \qquad (3.4)$$

Using the mean number of firings $\Lambda(t)$ of each neuron per second μ_i is written as,

$$\mu_i = n\Delta\Lambda(t_i), \qquad (3.5)$$

where Δ is the width of the bin. The density function $f(t)$ is defined by normalizing the intensity function $\Lambda(t)$. BARS approximate this density function by a linear combination of cubic splines. In particular, $f(t)$ is written as

$$f(t) \equiv \frac{\Lambda(t)}{\int_0^T \Lambda(u)du} = \sum_{j=1}^{C+2} \beta_j b_j(t), \qquad (3.6)$$

where C is the number of knots of cubic splines, each of which are located at ξ_j ($j = 1, 2, \cdots, C$), $b_j(t)$ is the jth function in a cubic B-spline basis, and β_j is its coefficient. $\int_0^T \Lambda(u)du$ can be approximated using the total number of firings, divided by the number n of observed neurons. To obtain the unknown quantities C, ξ_j, and β_j, the reversible-jump Markov chain Monte Carlo technique is used (Green, 1995; Dimatteo et al., 2001). In this study, I utilized the source code for BARS implemented by Wallstrom et al. (2008). $n\Delta\Lambda(t)$ can be used as a smoothed function of the time histogram of firings. Smoothing with BARS can follow sudden changes in the time histogram of firings (Kass et al., 2005; Wallstrom et al., 2008).

For comparison, I also used a gaussian filter. The value of the bandwidth Δ_g of the gaussian filter can be determined arbitrarily. A large Δ_g yields a smooth time histogram of firings, although sudden changes in the time histogram of firings will be lost. Below, I used the value of Δ_g that maximizes the sum of nonlinearity S_{NL}, which will be defined in section 4. As also used in Figures 2C and 2D, S_{NL} takes large positive values when the dynamics are chaotic. Therefore, this condition for determining Δ_g is expected to facilitate identification of chaotic properties of the dynamics. The dependence of S_{NL} on Δ_g for RSC and SSC, is shown in Figure 5A and 5B, respectively. The positions of Δ_g^* and Δ^* are shown with vertical arrows. It is observed that Δ_g^* and Δ^* do not coincide. The dependence of Δ_g^* on n with various N for RSC and SSC, is shown in Figure 5C and 5D, respectively. Similar to Δ^* shown in Figures 3C and 3D, Δ_g is also seen to increase with the decrease of n. Moreover, Δ_g largely fluctuates for $n \leq 100$, because S_{NL} becomes very small for $n \leq 100$, and consequently, the position of the peak of S_{NL} fluctuates markedly (Please see section 4).

In Figure 4, the smoothed time histograms of firings are shown; the time histogram of firings smoothed with BARS follows both rapid changes and slow changes in chaotic dynamics. In contrast, the time histogram of firings smoothed with a gaussian filter does not trace the original time histogram of firings, although it successfully removes the high frequency components from the time histogram of firings.

Using this result of smoothing with BARS, I confirm the validity of the assumption that k_i obeys a Poisson distribution with mean μ_i. Note that μ_i is not stationary and μ_i is not reproducible because dynamics treated in the study are chaotic. Instead of reproducing μ_i, I collect similar dynamical states. As shown in Figure 6A, I focus on local minima in a range $[\mu, \mu + d\mu]$, and collect k_i in this range. In order to confirm the validity of the assumption, a limit $d\mu \to 0$ should be considered. However, the number of bins that satisfy $\mu_i \in [\mu, \mu + d\mu]$ would be zero in the limit of $d\mu \to 0$. Therefore, we set $d\mu = 0.2$ in order to obtain sufficient number of bins. Distributions of k_i for $\mu = 1$ and $\mu = 7$ are shown in Figure 6B. Poisson distributions with $\mu = 1$ and $\mu = 7$ are also shown with open and filled circles, respectively. It is observed that k_i obeys a Poisson distribution although its shape is not smooth enough because the number of data is small.

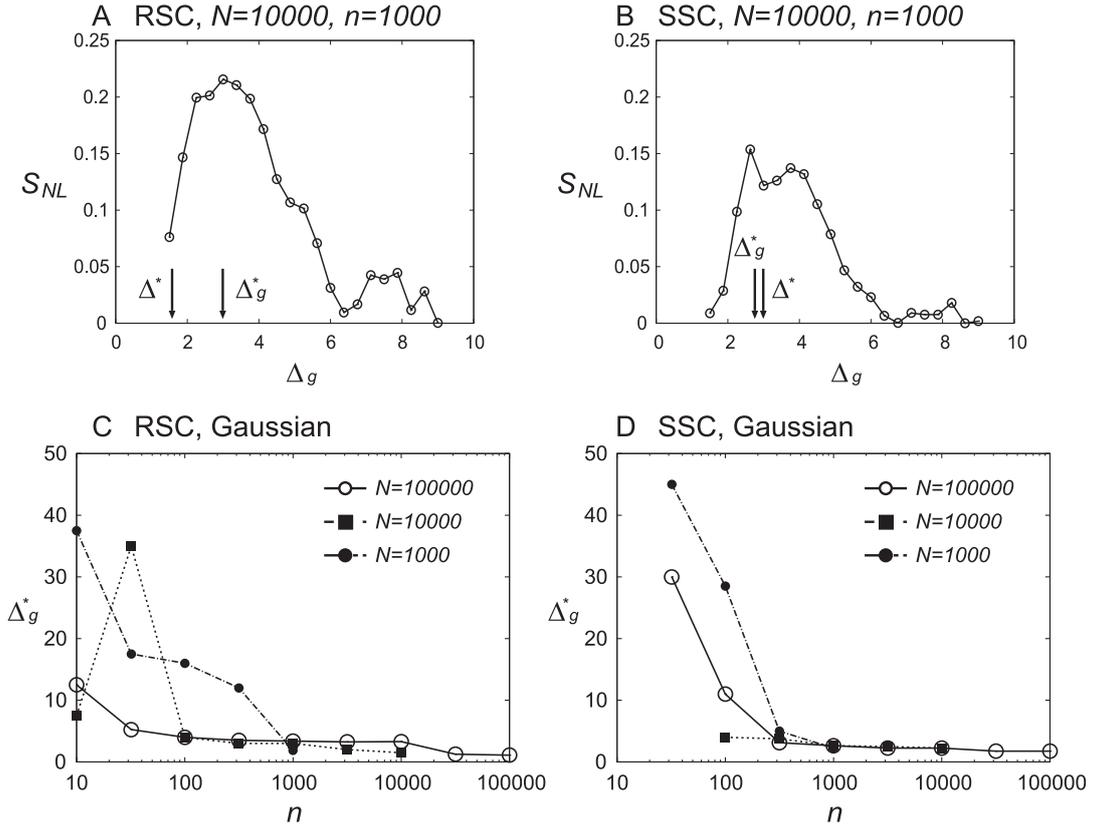In the next section, I consider the strength of chaos in the

Figure 5: Dependence of the sum of nonlinearity S_{NL} on the bandwidth Δ_g of the gaussian filter for (A) RSC and (B) SSC. The optimal bandwidth Δ_g^* is defined as the value that maximizes S_{NL}. Dependences of the optimal bandwidth Δ_g^* on n with various N for (C) RSC and (D) SSC.

smoothed time histogram of firings.

4 Quantifying the strength of chaos based on nonlinear prediction

4.1 Definition of the sum of nonlinearity

Using the smoothed time histogram of firings, I can calculate the ith peak time t_i and the IPI $T_i \equiv t_{i+1} - t_i$. To quantify the strength of chaos, a sequence $\{T_i\}$ of IPIs comprising about 1000 IPIs is required. However, 1000 IPIs cannot be directly prepared from a long time histogram of firings, because smoothing with BARS is unstable for such histograms. Therefore, I divided the long time histogram of firings into short time histograms of firings in the range of $[t_i^{(b)}, t_{i+1}^{(b)}]$ with $t_{i+1}^{(b)} = t_i^{(b)} + T_i^{(b)}$ and $T_i^{(b)} \leq 200$, as shown in Figure 4. Smoothing with BARS was then applied to each short time histogram of firings, and these histograms were then connected and the IPI sequence $\{T_i\}$ calculated. The borders $t_i^{(b)}$ $(i = 0, 1, 2 \cdots)$ of the short time histogram of firings were determined as follows. First, I set $t_0^{(b)} = 0$. $t_i^{(b)}$ $(i \geq 1)$ were determined as the time at which the histogram was minimized in the range $t_{i-1}^{(b)} + 50 \leq t \leq t_{i-1}^{(b)} + 200$. For the data in Figure 1A, $t_i^{(b)}(i \geq 1)$ were calculated as

$\{124.5, 201.0, 306.0, 387.0, \cdots\}$.

In contrast, smoothing with a gaussian filter could be applied directly to the long time histogram of firings. The dependence of computation time of smoothing with BARS and with a gaussian filter on the number L of bins is shown in Figure 7. The calculations were performed using a single core of Intel Xeon (E5-1650, 3.60 GHz) for various N and n. All the data in Figure 7 were obtained during the quantification of the strength of chaos that are shown in Figures 11 and 14 in section 4. In Figure 7A, the computation time for smoothing with BARS is shown. This time includes the computation times for smoothing the many short time histograms. In Figure 7B, the mean computation time for smoothing the short time histograms of firings with BARS is shown, which was obtained by dividing both the computation time and L by M, for M short time histograms. Note that Figures 7A and 7B show semi-log graphs. Figures 7A and 7B also show the fit with an exponential function and with a linear function, and their coefficients of determination R^2. It was observed that the computation time for smoothing with BARS increased exponentially with the increase of L. The computation time for smoothing with a gaussian filter is shown in Figure 7C, which can be seen to increase linearly with the increase of L.

In this study, I applied the nonlinear prediction method, based on reconstruction of the IPI sequence $\{T_i\}$, to quan-
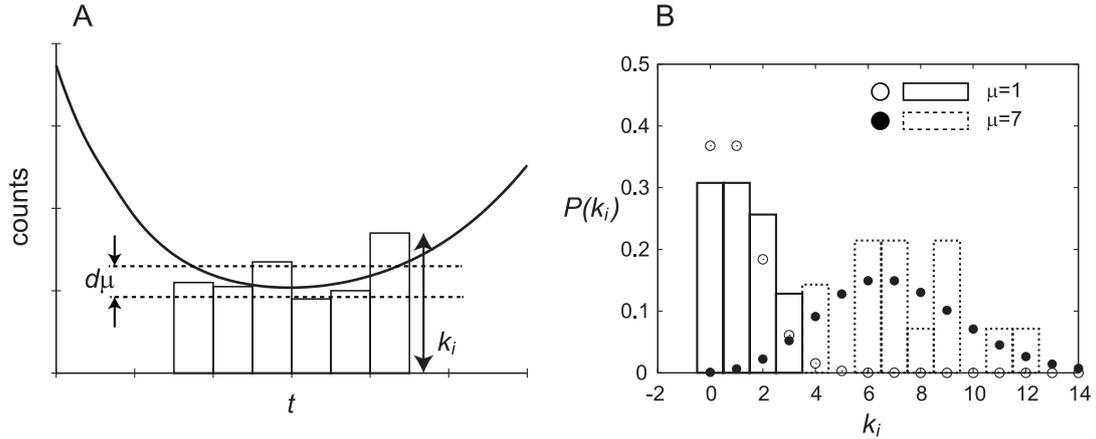
Figure 6: (A) A schematic diagram for choosing bins around local minima in a range $[\mu, \mu + d\mu]$. (B) Distributions of k_i and Poisson distributions with $\mu = 1$ and 7.

tify the strength of chaos (Theiler et al., 1992; Sauer, 1994) (Appendix B). In this method, if the prediction error takes large values, the sequence is regarded as being generated by some stochastic process, whereas if the prediction error is small, it can be concluded that the sequence may contain deterministic structures, such as strange attractors. Moreover, the prediction was applied to surrogate data generated from the original time series; by comparing these results with those obtained from the original data, I examined the type of stochastic process that generated the original data set.

The surrogate data were generated from the original time series under certain null hypotheses, such that the new time series preserved some of the statistical properties of the original data. In this study, I used two types of surrogates: randomly shuffled (RS) and amplitude-adjusted Fourier transformed (AAFT) surrogate data. RS surrogate data correspond to the null hypothesis that the data are generated from an independent and identically distributed random process. AAFT surrogate data correspond to the null hypothesis that the data are generated from a linear stochastic process observed via a monotonic nonlinear function.

I calculated the nonlinear prediction error $E_{NP}(h)$ for the prediction step h for both the original and surrogate data. The exact definition of $E_{NP}(h)$ is given in Appendix B. I generated 100 samples of surrogate data and calculated $E_{NP}(h)$, its mean $\mu(h)$, and standard deviation $\sigma(h)$.

First, in order to confirm that $E_{NP}(h)$ for 100 samples of surrogate data follows a gaussian distribution, I drew distributions of $E_{NP}(h)$ with $h = 1$ for RS and AAFT surrogate data for $N = 10,000$ and $n = 1000$ and for $N = n = 10,000$ in Figures 8A and 8B, respectively. To test their normality, I performed D'Agostino and Pearson's (1973) test. The obtained p-values are also shown in Figures 8A and 8B. It is observed that all the p-values are larger than a significance level of 0.05; therefore, a null hypothesis that $E_{NP}(1)$ follows a normal distribution cannot be rejected, and I cannot conclude $E_{NP}(1)$ do not follow a normal distribution. Moreover, I also drew the corresponding QQ-plot and lines that connect the first and the third quartiles in Fig-

ures 8C and 8D. Linear relations of QQ-plots also show the normality of $E_{NP}(1)$. Similarly, it can be confirmed that $E_{NP}(h)$ for $h > 1$ also follows a gaussian distribution.

Then the 95% confidence interval of $E_{NP}(h)$ is $[\mu(h) - 1.96\sigma(h), \mu(h) + 1.96\sigma(h)]$. If a value of h exists where $E_{NP}(h)$ of the original data falls outside of the confidence interval of $E_{NP}(h)$ of the surrogate data, I judged that $E_{NP}(h)$ of the original data and that of the surrogate data differ significantly from each other. In such a case, I rejected the null hypothesis, and concluded that it was possible that the original time series contained deterministic structures, such as strange attractors.

In contrast, if $E_{NP}(h)$ obtained for the surrogate data did not differ significantly from that obtained for the original data, the null hypothesis is not rejected, and the original data are regarded as being generated by some stochastic process.

$E_{NP}(h)$ obtained for the IPI sequence $\{T_i\}$ of the smoothed time histogram of firings of RSC with BARS, for $N = 10,000$, $n = 1000$, and $\Delta = \Delta^* = 1.5$ (Figure 1A) is shown in Figure 9A, denoted as "org". The mean $\mu(h)$ of $E_{NP}(h)$ for 100 samples of surrogate data (RS and AAFT) is also shown with filled and open circles, respectively. The data for the two types of surrogate data have almost identical values, and the filled and open circles almost cover each other. The 95% confidence intervals of $E_{NP}(h)$ for each surrogate data set are also shown with error bars, but these are narrower than the filled and open circles. For example, the 95% confidence intervals for $h = 1$ are $[1.004, 1.019]$ and $[1.000, 1.016]$ for the RS and AAFT surrogate data, respectively. $E_{NP}(h)$ for the RS and AAFT surrogate data exhibited significant differences, compared to those values for the original data, although the two kinds of surrogate data had almost identical values and the filled and open circles almost cover each other. This suggested that deterministic structures were present in the original sequence $\{T_i\}$. Sensitive dependence on the initial conditions was also suggested, because $E_{NP}(h)$ increased monotonically as the prediction step h increased. Moreover, the return plot for $\{T_i\}$ in the inset of Figure 9A had two decreasing sections, similar to that in
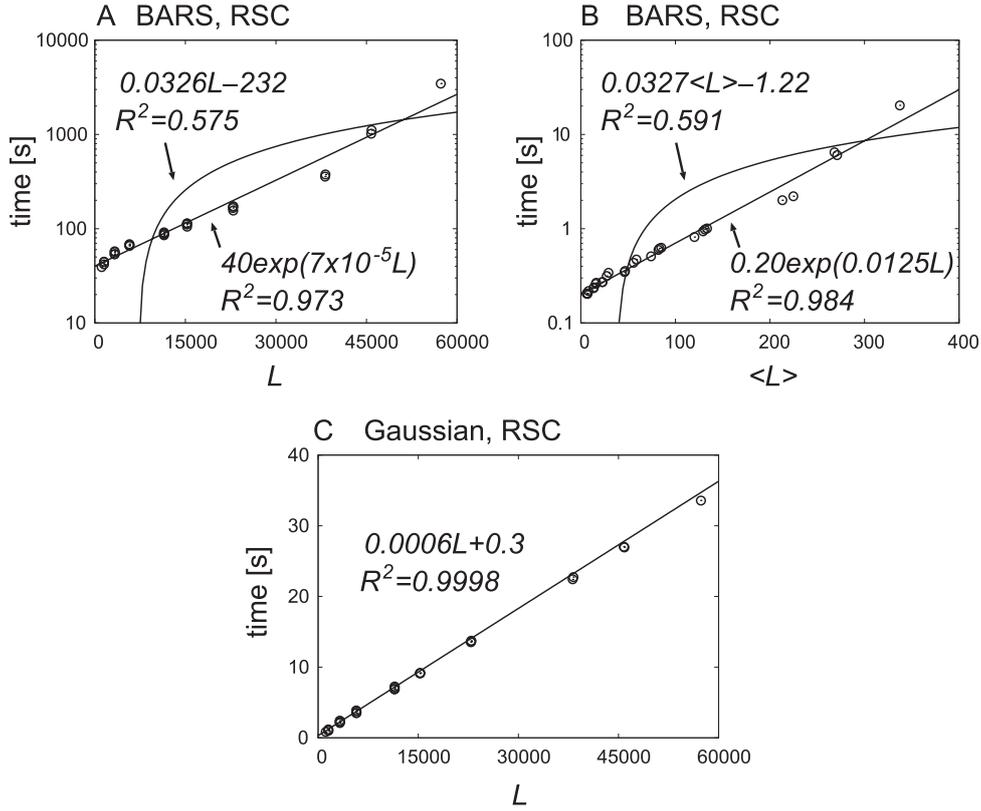
Figure 7: Dependence of the computation time of smoothing on the number L of bins. The data, calculated with various N and n, used in Figures 11 and 14 are plotted. Note that panels A and B show semi-log graphs. (A) Computation time for smoothing with BARS. (B) Mean computation time for smoothing the short-time histogram of firings with BARS. (C) Computation time for smoothing with a gaussian filter.

Figure 2C, although the decreasing section for $28 < T_i < 43$ was highly irregular.

To quantify the strength of chaos, I also show $E_{NP}(h)$ for $N = n = 10,000$ with $\Delta = \Delta^* = 0.6$, in Figure 9B. It can be assumed that the strength of chaos in the time sequence shown in Figure 9B is larger than that in Figure 9A because a large n would be able to retain any chaotic properties that exist in the original dynamics of N neurons. It was observed that the difference between $E_{NP}(h)$ of the original time series and that of the surrogate data (RS and AAFT) was slightly larger than that in Figure 9A; therefore, this difference can act as a measure to quantify the strength of chaos. Note that this difference is also affected by the bin size Δ. However, in this study, I attempted to find a method for quantifying the strength of chaos under the condition where Δ is set to the value Δ^* that minimizes $C(\Delta)$.

To quantify the strength of chaos, I defined the sum of nonlinearity (Kanamaru & Aihara, 2012). The definition of the sum of nonlinearity in this study is slightly modified from that in Kanamaru & Aihara (2012), in order to improve its statistical plausibility. Note that the behaviors of the two versions of the sum of nonlinearity are quite similar. First, I defined the 95% confidence intervals of $E_{NP}(h)$ for the RS and AAFT surrogate data as $\left[c_{min}^{RS}(h), c_{max}^{RS}(h)\right]$ and $\left[c_{min}^{AAFT}(h), c_{max}^{AAFT}(h)\right]$, respectively. Then, the sum of

nonlinearity was defined as

$$S_{NL} = \sum_{h=1}^{10} \Theta(\min(c_{min}^{RS}(h), c_{min}^{AAFT}(h)) - E_{NP}(h)), \quad (4.1)$$

$$\min(x, y) = \begin{cases} x & (x < y) \\ y & (x \geq y) \end{cases}, \quad (4.2)$$

$$\Theta(x) = \begin{cases} x & (x \geq 0) \\ 0 & (x < 0) \end{cases}. \quad (4.3)$$

The values of S_{NL} are shown in each panel of Figure 9. I used S_{NL} to quantify the strength of chaos in the time series of ensemble-averaged firing rates. Although there is no correspondence to other quantities to measure the strength of chaos, such as the largest Lyapunov exponent (Ott, 2002), S_{NL} has the advantage that it can be calculated from the IPI sequences only and does not require information about the system. Therefore, S_{NL} satisfies the first condition for quantifying the strength of chaos as stated in section 1—the method quantifies the strength of chaos from spiking data alone. If S_{NL} is zero, the data can be regarded as being generated by a stochastic process, and if S_{NL} takes a large positive value, there is a possibility that chaos may exist in the system.

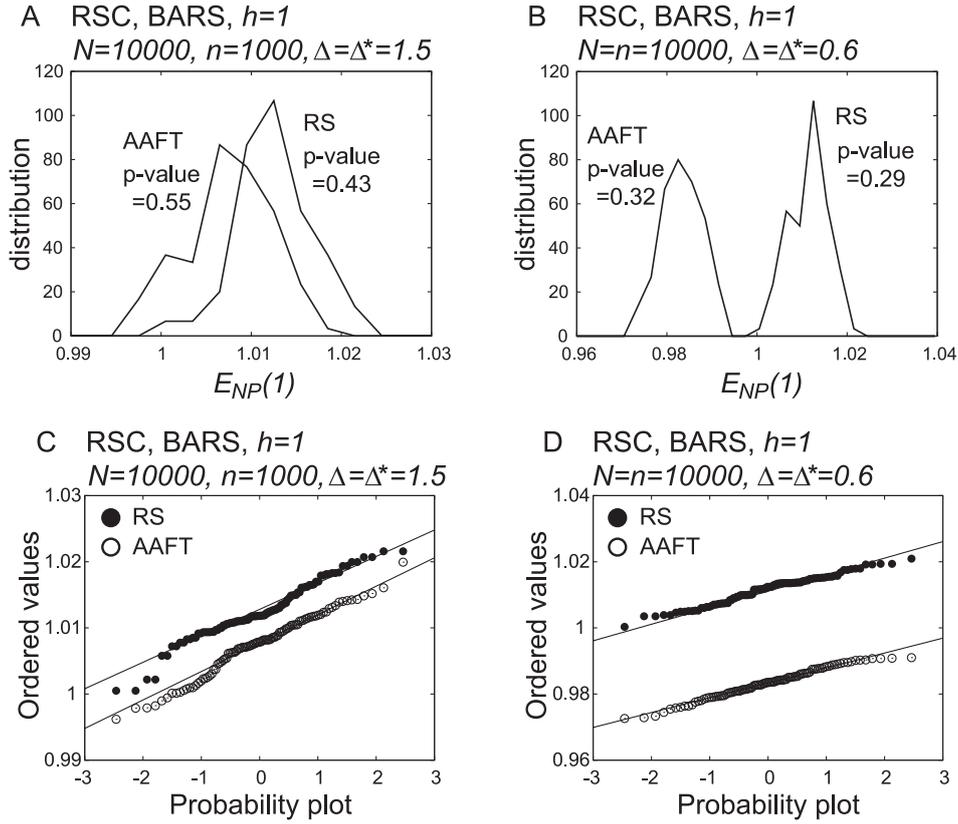Kanamaru & Aihara (2012) used the slightly modified ver-

9

Figure 8: (A, B) Distributions of $E_{NP}(h)$ with $h = 1$ for 100 samples of surrogate data (RS and AAFT) for $N = 10,000$ and $n = 1000$ and for $N = n = 10,000$. p-values obtained by D'Agostino and Pearson's test are also shown. (C, D) The corresponding QQ-plots of $E_{NP}(h)$ with $h = 1$. All the plots show that $E_{NP}(h)$ follows a gaussian distribution.

sion of S_{NL}:

$$N_{sum} = \sum_{h=1}^{10} \Theta(E_{NP}^{AAFT}(h) - \sigma^{AAFT}(h) - E_{NP}(h)).$$

(4.4)

The relationship between N_{sum} and S_{NL} in Figure 10 shows a linear relation. All the data in Figure 10 were obtained
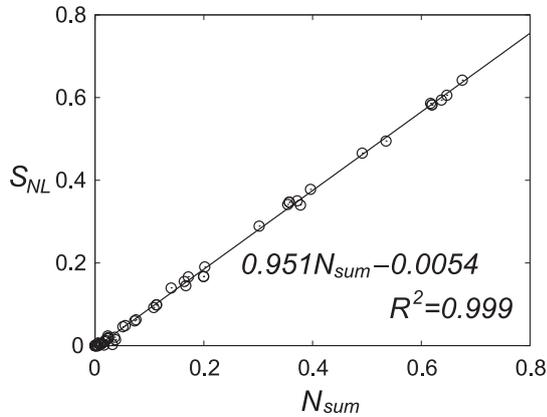

Figure 10: The relationship between two versions of sum of nonlinearity. A linear relation is observed.

for the parameters that will be used in Figures 11 and 14. In Kanamaru & Aihara (2012), for noisy chaotic sequences, N_{sum} took values in a range $[0.3, 3]$, which was typical "large" values of N_{sum}. Therefore, it is expected that S_{NL} also takes similar values for chaotic sequences. Note that a range $[0.3, 3]$ was presented here just as a guide. A criterion of "large" S_{NL} should be obtained by experiments for various systems.

Note that both $E_{NP}(h)$ and S_{NL} depend on the width Δ of the bin. $E_{NP}(h)$ for $\Delta = 0.1$ and 3.0 are shown in Figure 9C and 9D, respectively. The values for the other parameters are identical to those of Figure 9A. It was observed that $E_{NP}(h)$ and S_{NL} depend on Δ. Therefore, a careful choice of Δ is required. In this work, the method for determining Δ proposed by Shimazaki & Shinomoto (2007) was used.

4.2 Quantifying the strength of chaos

Below, I shorten "S_{NL} of the time histogram smoothed using BARS and a gaussian filter" to "S_{NL} with BARS and a gaussian filter". Similarly, I use the shortened term "S_{NL} without smoothing" to indicate S_{NL} that is applied to the instantaneous firing rate in the limit of $N \to \infty$, because smoothing is not required in such a case.

The dependence of S_{NL} for RSC on the number N of neurons is shown in Figure 11A. The number n of excitatory
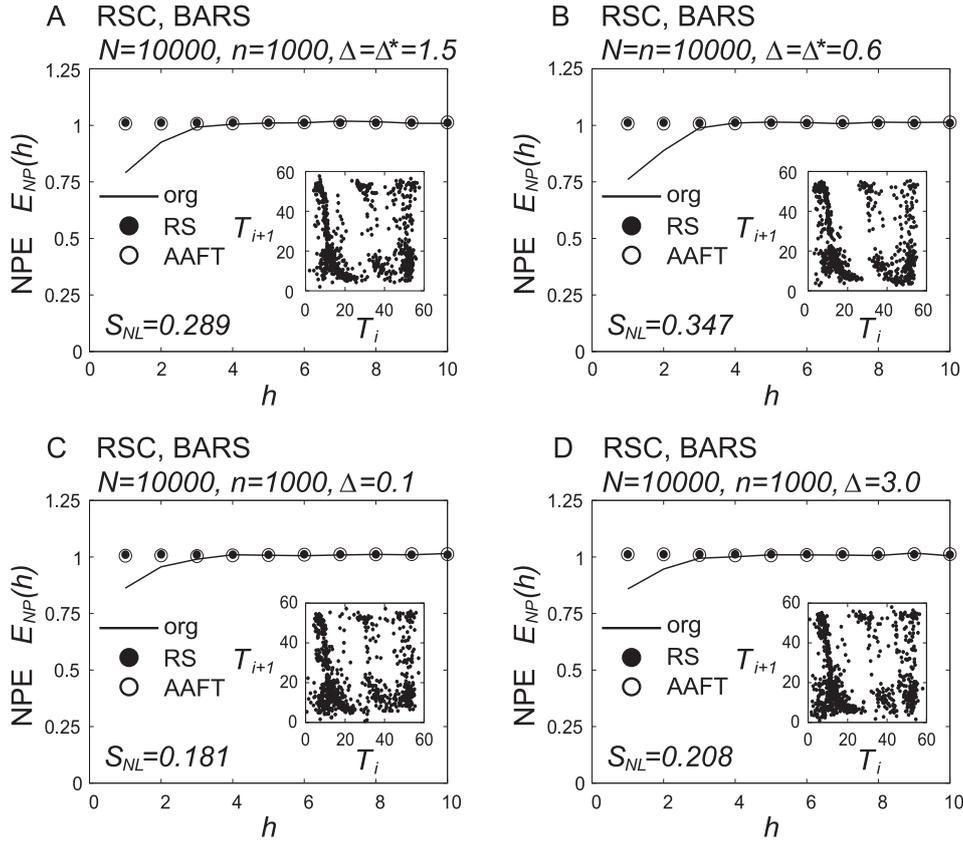
Figure 9: (A) Analysis using the nonlinear prediction method for the IPI sequence $\{T_i\}$ of the time histogram of firings smoothed with BARS for RSC, with $N = 10,000$, $n = 1000$, $\Delta = \Delta^* = 1.5$. $E_{NP}(h)$ for the original time series are shown with solid lines and denoted as "org". Mean values for 100 samples of surrogate data (RS and AAFT) are also shown with filled and open circles. The 95% confidence intervals of surrogate data are also shown as error bars, but they are narrower than the size of the filled and open circles. The inset shows the return plot for $\{T_i\}$, which has a similar structure to that in Figure 2C. (B) Result for $N = n = 10,000$ and $\Delta = \Delta^* = 0.6$. (C) Result for $N = 10,000$, $n = 1000$, and $\Delta = 0.1$. (D) Result for $N = 10,000$, $n = 1000$, and $\Delta = 3.0$.

neurons observed was set to $n = N$. Both S_{NL} with BARS and a gaussian filter are shown.

Both sets of results show that S_{NL} was large for a sufficiently large N, and it decreased with the decrease of N. This result seems intuitively plausible, because RSC is confirmed to be chaotic in the limit of $N \to \infty$, and this chaos would be lost with the decrease of N because of its finite-size effect. For comparison, in the limit of $N \to \infty$, I calculated S_{NL} without smoothing for the data shown in Figure 2A as 1.762. It would be expected that the rate of increase of S_{NL} with the increase of N in Figure 11A becomes moderate and S_{NL} converges to 1.762 in the limit of $N \to \infty$. Therefore, I concluded that both S_{NL} with BARS and with a gaussian filter satisfies the second condition for quantifying the strength of chaos stated in section 1—that the strength of chaos obtained by the proposed method should take large values when applied to firings that are confirmed to be chaotic.

To examine the properties of S_{NL}, the distributions of S_{NL} for various parameters were investigated and are shown in Figure 12. Each distribution was calculated from 100 S_{NL}, obtained by performing 100 simulations of equations

2.1 and 2.2. Figures 12A and 12B show the distributions for BARS and the gaussian filter, respectively. Both results show that the distribution becomes narrow for small S_{NL}. Moreover, the results for 500 IPIs are also shown, and are labeled as "#IPI=500", while other results were calculated for 1000 IPIs. It can be observed that a small number of IPIs broaden the distribution of S_{NL}. Note that the analysis shown in Figure 12 is possible for theoretical models because many IPIs can be produced by simulations. For experimental data with only a single sequence of IPIs, only one value of S_{NL} is obtained. A bootstrapping of the sequence of IPIs will not work because S_{NL} depends on the temporal correlation of the IPIs and the bootstrapping will break this correlation.

Similarly, I quantified the strength of chaos in SSC. It is expected that S_{NL} for SSC is smaller than that for RSC, to reflect the values of S_{NL} without smoothing in the limit of $N \to \infty$, shown in Figures 2C and 2D. The dependence of S_{NL} on N, with $n = N$, is shown in Figure 11B. It can be observed that S_{NL} with BARS for SSC took smaller values than that for RSC. In contrast, S_{NL} with a gaussian filter for SSC took larger values than that for RSC. To facilitate
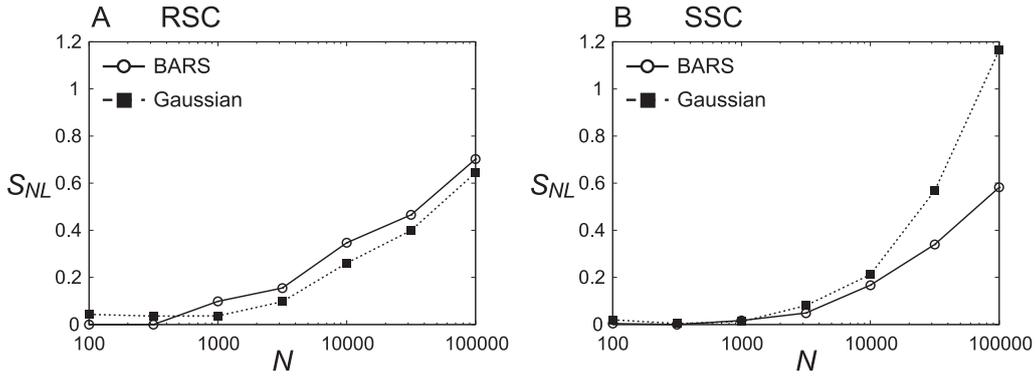
Figure 11: Dependence of the sum of nonlinearity S_{NL} on the number N of neurons. Both S_{NL} with BARS and a gaussian filter are shown. (A) Result for RSC. (B) Result for SSC.
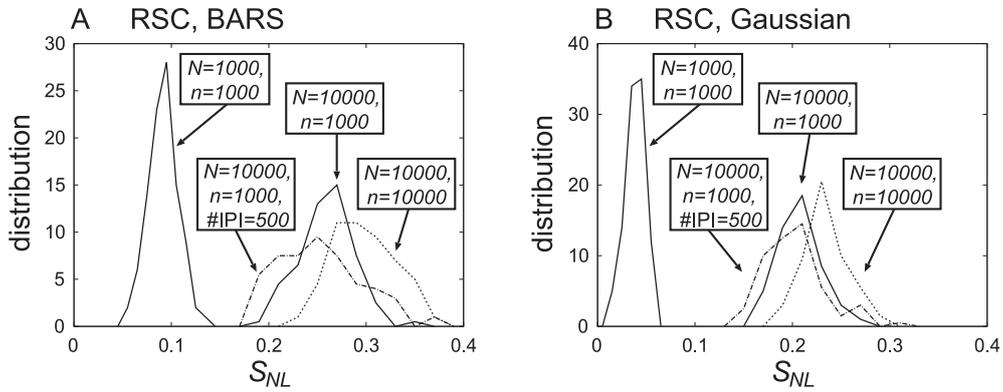

Figure 12: Distributions of S_{NL} for various parameters. Each distribution was calculated from 100 S_{NL} obtained by performing 100 simulations of equations 2.1 and 2.2. (A) Distributions of S_{NL} with BARS. (B) Distributions of S_{NL} with a gaussian filter.

understanding of this phenomenon, power spectra of the instantaneous firing rates of RSC and SSC, shown in Figures 2A and 2B in the limit of $N \to \infty$, are shown in Figure 13. It can be observed that the power of SSC is concentrated in a
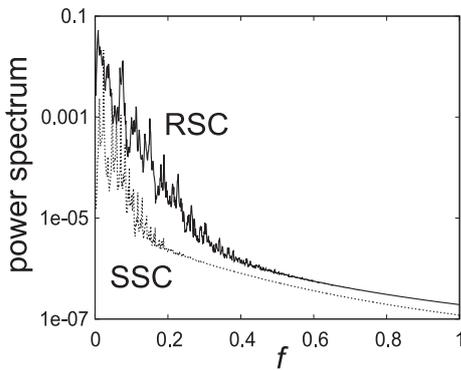

Figure 13: Power spectra of the instantaneous firing rates of RSC and SSC shown in Figures 2A and 2B in the limit of $N \to \infty$.

low-frequency region. Therefore, the effect of low-pass fil-

tering by the gaussian filter works more effectively on SSC than on RSC. Based on this result, I concluded that S_{NL} with the gaussian filter does not satisfy the third condition for quantifying the strength of chaos stated in section 1— that the strength of chaos obtained by the proposed method should reflect the strength of chaos of the original dynamics. As shown in Figure 2C and 2D, in the limit of $N \to \infty$, S_{NL} without smoothing for SSC (1.509) is smaller than that for RSC (1.762). Therefore, it is preferable that S_{NL} for SSC is smaller than that for RSC. Only S_{NL} with BARS satisfies this condition.

Next, the dependence of S_{NL} for RSC on the number n of excitatory neurons observed is shown in Figures 14A and 14C. S_{NL} with BARS and the gaussian filter, are shown in Figures 14A and 14C, respectively. As shown in Figure 14A, S_{NL} decreased as n decreased. It was also clear that the results obtained with large values of N had large values of S_{NL}; this was the case even for small values of n. These results also seem intuitively plausible because chaos will be lost as the number n of observed neurons decreases. This also suggests that S_{NL} with BARS satisfies the third condition for quantifying the strength of chaos stated in section 1. The dependence of S_{NL} on n for SSC is shown in Figures
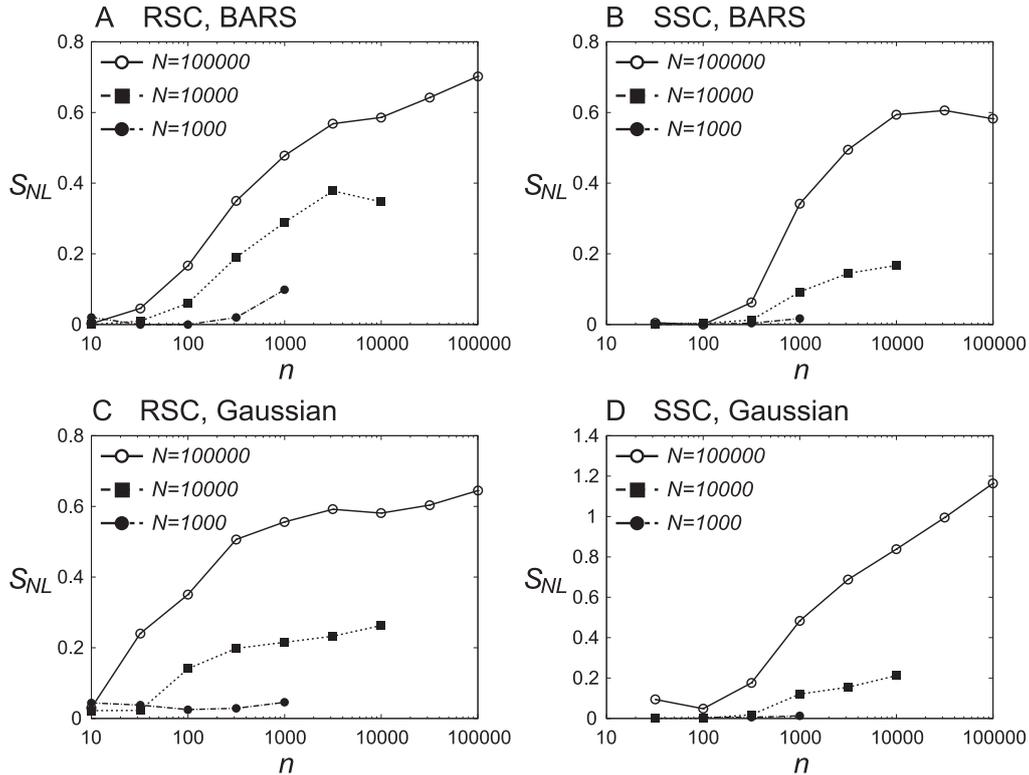
Figure 14: Dependence of the sum of nonlinearity S_{NL} on the number n of excitatory neurons observed for (A, C) RSC and (B, D) SSC. (A, B) S_{NL} with BARS. (C, D) S_{NL} with a gaussian filter.

14B and 14D. Similar dependence of S_{NL} was observed.

5   Conclusions

In this study, I quantified the strength of chaos in the population firing rate of a pulse-coupled neural network. N excitatory neurons and N inhibitory neurons comprised the network, and I observed the firing of n excitatory neurons. I defined two classes of chaotic firing, RSC and SSC. RSC refers to firing where the population firing rate is chaotic and the firing of each neuron is stochastic. SSC is a special case of RSC, where the firing rate of each neuron is much lower than that in RSC. First, I calculated the time histogram of firings to show the variation in the population firing rate for n excitatory neurons over time. I employed BARS and a gaussian filter to smooth the time histogram of firings. To quantify the strength of chaos in the smoothed time histogram of firings, I used a nonlinear prediction method based on reconstruction, and I defined the sum of nonlinearity S_{NL}. I examined the dependence of S_{NL} on N and n. I demonstrated that S_{NL} with BARS satisfies three properties for quantifying the strength of chaos. First, it can be calculated from spiking data only. Second, it takes large values when applied to firings that are confirmed to be chaotic, either theoretically or numerically. Third, it reflects the strength of chaos of the original dynamics.

Note that this conclusion depends on the choice of the bin size Δ in the time histogram. When arbitrarily chosen values of Δ are used, even S_{NL} with BARS would lose the above properties. Similarly, the choice of the values of Δ and Δ_g are also important for S_{NL} with the gaussian filter. If an appropriate method for determining Δ and Δ_g are found, even S_{NL} with the gaussian filter would satisfy the above properties. In this study, I found that the method for determining Δ as proposed by Shimazaki & Shinomoto (2007) made it possible to quantify the strength of chaos appropriately using S_{NL} with BARS. I think that this property was realized by the fact that the optimal Δ^* minimizes the mean integrated squared error between the underlying spiking rate and the its estimator (Shimazaki & Shinomoto, 2007). However, further studies would be required to verify this assumption.

I used BARS as a smoothing method in order to follow sudden changes in the time histogram of firings. Comparison with other methods for estimating the time-varying firing rate, such as the multiscale analysis (Ramezan et al., 2014), is a future prospect.

When N is excessively small, the strength of chaos would become small, because chaos breaks due to the finite-size effect. In contrast, if N is sufficiently large, it might be possible to find chaos even when the number n of excitatory neurons observed is small. In fact, as shown in Figure 14A, a somewhat large S_{NL} was observed with $N = 10,0000$ and $n = 100$. For physiological experiments, it is important to develop a method for finding chaos at smaller values of n. To that end, it might be effective to utilize firing over a much

13

longer range of time. The development of this method will be addressed in future research.

A Fokker-Planck equation

To analyze the average dynamics of the network, I use the Fokker-Planck equations (Kanamaru & Aihara, 2008), which are written as

$$
\begin{aligned}
\frac{\partial n_E}{\partial t} &= -\frac{\partial}{\partial \theta_E}(A_E n_E) \\
&\quad + \frac{D}{2}\frac{\partial}{\partial \theta_E}\left\{B_E\frac{\partial}{\partial \theta_E}(B_E n_E)\right\}, \quad (A.1) \\
\frac{\partial n_I}{\partial t} &= -\frac{\partial}{\partial \theta_I}(A_I n_I) \\
&\quad + \frac{D}{2}\frac{\partial}{\partial \theta_I}\left\{B_I\frac{\partial}{\partial \theta_I}(B_I n_I)\right\}, \quad (A.2) \\
A_E(\theta_E, t) &= (1-\cos\theta_E) + (1+\cos\theta_E) \\
&\quad \times (r_E + g_{EE}I_E(t) - g_{EI}I_I(t)), (A.3) \\
A_I(\theta_I, t) &= (1-\cos\theta_I) + (1+\cos\theta_I) \\
&\quad \times (r_I + g_{IE}I_E(t) - g_{II}I_I(t) \\
&\quad + g_{gap}I_{gap}(\theta_I, t)), \quad (A.4) \\
B_E(\theta_E, t) &= 1 + \cos\theta_E, \quad (A.5) \\
B_I(\theta_I, t) &= 1 + \cos\theta_I, \quad (A.6) \\
I_{gap}(\theta_I, t) &= \langle\sin\theta_I\rangle\cos\theta_I - \langle\cos\theta_I\rangle\sin\theta_I, (A.7) \\
\langle f(\theta_I)\rangle &= \int_0^{2\pi} f(\theta_I)\, n_I(\theta_I, t)\, d\theta_I, \quad (A.8)
\end{aligned}
$$

for the normalized number densities of excitatory and inhibitory ensembles, in which

$$
\begin{aligned}
n_E(\theta_E, t) &\equiv \frac{1}{N}\sum\delta(\theta_E^{(i)} - \theta_E), \quad (A.9) \\
n_I(\theta_I, t) &\equiv \frac{1}{N}\sum\delta(\theta_I^{(i)} - \theta_I), \quad (A.10)
\end{aligned}
$$

in the limit of $N \to \infty$. The probability flux for each ensemble is defined as

$$
\begin{aligned}
J_E(\theta_E, t) &= A_E n_E - \frac{D}{2}B_E\frac{\partial}{\partial \theta_E}(B_E n_E), (A.11) \\
J_I(\theta_I, t) &= A_I n_I - \frac{D}{2}B_I\frac{\partial}{\partial \theta_I}(B_I n_I), \quad (A.12)
\end{aligned}
$$

respectively. The probability flux at $\theta = \pi$ can be interpreted as the instantaneous firing rate in this ensemble, which is denoted as $J_X(t) \equiv J_X(\pi, t)$ where $X = E$ or I.

$I_X(t)$ in equation 2.3 follows a differential equation that is written as

$$
\dot{I_X}(t) = -\frac{1}{\kappa_X}\left(I_X(t) - \frac{1}{2}J_X(t)\right). \quad (A.13)
$$

In order to integrate the Fokker-Planck equations A.1 and A.2 numerically, I expanded $n_E(\theta_E, t)$ and $n_I(\theta_I, t)$ into Fourier series as

$$
\begin{aligned}
n_E(\theta_E, t) &= \frac{1}{2\pi} \\
&\quad + \sum_{k=1}^{\infty}(a_k^E(t)\cos(k\theta_E) + b_k^E(t)\sin(k\theta_E)), \quad (A.14) \\
n_I(\theta_I, t) &= \frac{1}{2\pi} \\
&\quad + \sum_{k=1}^{\infty}(a_k^I(t)\cos(k\theta_I) + b_k^I(t)\sin(k\theta_I)), \quad (A.15)
\end{aligned}
$$

and, by substituting them, equations A.1 and A.2 were transformed into a set of ordinary differential equations of a_k^X and b_k^X, which are written as

$$
\begin{aligned}
\frac{da_k^{(X)}}{dt} &= -(r_X + \tilde{I}_X + 1)\frac{k}{\tau_X}b_k^{(X)} \\
&\quad -(r_X + \tilde{I}_X - 1)\frac{k}{2\tau_X}(b_{k-1}^{(X)} + b_{k+1}^{(X)}) \\
&\quad -\frac{Dk}{8\tau_X^2}f(a_k^{(X)}) \\
&\quad +\frac{\pi g_{gap}k}{4\tau_X}(-b_1 g_1(b_k^{(X)}) + a_1 g_2(a_k^{(X)}))\delta_{XI}, \\
&\quad\quad\quad (A.16) \\
\frac{db_k^{(X)}}{dt} &= (r_X + \tilde{I}_X + 1)\frac{k}{\tau_X}a_k^{(X)} \\
&\quad +(r_X + \tilde{I}_X - 1)\frac{k}{2\tau_X}(a_{k-1}^{(X)} + a_{k+1}^{(X)}) \\
&\quad -\frac{Dk}{8\tau_X^2}f(b_k^{(X)}) \\
&\quad +\frac{\pi g_{gap}k}{4\tau_X}(b_1 g_1(a_k^{(X)}) + a_1 g_2(b_k^{(X)}))\delta_{XI}, \\
&\quad\quad\quad (A.17) \\
f(x_k) &= (k-1)x_{k-2} + 2(2k-1)x_{k-1} + 6kx_k \\
&\quad + 2(2k+1)x_{k+1} + (k+1)x_{k+2}, \quad (A.18) \\
g_1(x_k) &= x_{k-2} + 2x_{k-1} + 2x_k + 2x_{k+1} + x_{k+2}, \\
&\quad\quad\quad (A.19) \\
g_2(x_k) &= x_{k-2} + 2x_{k-1} - 2x_{k+1} - x_{k+2}, \quad (A.20) \\
\tilde{I}_X &\equiv g_{XE}I_E - g_{XI}I_I, \quad (A.21) \\
a_0^{(X)} &\equiv \frac{1}{\pi}, \quad (A.22) \\
b_0^{(X)} &\equiv 0, \quad (A.23) \\
a_{-n}^{(X)} &\equiv a_n^{(X)}, \quad (A.24) \\
b_{-n}^{(X)} &\equiv -b_n^{(X)}, \quad (A.25)
\end{aligned}
$$

where $X = E$ or I. By integrating the ordinary differential equations A.13, A.16, and A.17 numerically, the time series of the probability fluxes J_E and J_I are obtained. For numerical calculations, each Fourier series was truncated at the first 40 terms.

14

B Nonlinear prediction based on reconstruction

In this section, the nonlinear prediction method based on reconstruction of dynamics is summarized (Theiler et al., 1992; Sauer, 1994).

Let us consider a sequence $\{T_k\}$ of the duration of patterns and the delay coordinate vectors $V_j = (T_{j-m+1}, T_{j-m+2}, \ldots, T_j)$ with the reconstruction dimension m, and let L be the number of vectors in the reconstructed phase space $\boldsymbol{R}^m$. For a fixed integer j_0, I choose $l = \beta L$ ($\beta < 1$) points that are nearest to the point V_{j_0} and denote them by $V_{j_k} = (T_{j_k-m+1}, T_{j_k-m+2}, \ldots, T_{j_k})(k = 1, 2, \ldots, l)$. I set $\beta = 0.05$ in this study. It was confirmed that the value of β does not affect the results critically. Given $\{V_{j_k}\}$, a predictor of T_{j_0} for h steps ahead is defined as

$$p_{j_0}(h) = \frac{1}{l} \sum_{k=1}^{l} T_{j_k+h}. \qquad \text{(B.1)}$$

With $p_{j_0}(h)$, the normalized prediction error (NPE) is defined as

$$E_{NP}(h) = \frac{\langle (p_{j_0}(h) - T_{j_0+h})^2 \rangle^{1/2}}{\langle (\langle T_{j_0} \rangle - T_{j_0+h})^2 \rangle^{1/2}}, \qquad \text{(B.2)}$$

where $\langle \cdot \rangle$ denotes the average over j_0. A small value of $E_{NP}(h)$ i.e., less than 1, implies that the sequence has deterministic structure behind the time series because this algorithm is based on the assumption that the dynamical structure of a finite-dimensional deterministic system can be well reconstructed by the delay coordinates of the sequence (Sauer, 1994). However, stochastic time series with large autocorrelations can also take $E_{NP}(h)$ values less than 1. Therefore, I can not conclude that there is deterministic structure only from the magnitude of $E_{NP}(h)$.

To confirm the deterministic structure, the values of $E_{NP}(h)$ should be compared with those of $E_{NP}(h)$ for a set of surrogate data (Theiler et al., 1992). The surrogate data used in this study are new time series generated from the original time series under some null hypotheses so that the new time series preserve some statistical properties of the original data. In the present study, I use randomly shuffled (RS) and amplitude adjusted Fourier transformed (AAFT) surrogate data, which correspond to the null hypothesis of an independent and identically distributed random process and that of a linear stochastic process observed through a monotonic nonlinear function, respectively. To obtain AAFT surrogate data, I use TISEAN 3.0.1 (Hegger, Kantz, & Schreiber, 1999; Schreiber & Schmitz, 2000). If the values of $E_{NP}(h)$ for the original data are significantly smaller than those of $E_{NP}(h)$ for the surrogate data, the null hypothesis is rejected, and it can be concluded that there is some possibility that the original time series has deterministic structure.

References

Angulo-Garcia, D., & Torcini, A. (2014). Stable chaos in fluctuation driven neural circuits *Chaos, solitons & fractals*, *69*, 233 – 245.

Angulo-Garcia, D., & Torcini, A. (2015). Stochastic mean-field formulation of the dynamics of diluted neural networks. *Physical Review E*, *91*, 022928.

Brunel, N. (2000). Dynamics of sparsely connected networks of excitatory and inhibitory spiking neurons. *Journal of Computational Neuroscience*, *8*, 183–208.

Brunel, N., & Hansel, D. (2006). How noise affects the synchronization properties of recurrent networks of inhibitory neurons. *Neural Comput.*, *18*, 1066 – 1110.

Buzsáki, G., Horváth, Z., Urioste, R., Hetke, J., & Wise, K. (1992). High-frequency network oscillation in the hippocampus. *Science*, *256*, 1025 – 1027.

Conti, F., de Felice, L. J., &Wanke, E. (1975). Potassium and sodium ion current noise in the membrane of the squid giant axon. *Journal of Physiology*, *248*, 45 – 82.

Csicsvari, J., Hirase, H., Czurko, A., & Buzsáki, G. (1998). Reliability and state dependence of pyramidal cell-interneuron synapses in the hippocampus: an ensemble approach in the behaving rat. *Neuron*, *21*, 179 – 189.

D'Agostino, R., & Pearson, E. S. (1973). Tests for departure from normality. *Biometrika*, *60*, 613 – 622.

Dimatteo, I., Genovese, C. R., Kass, R. E. (2001). Bayesian curve-fitting with free-knot splines. *Biometrika*, *88*, 1055 – 1071.

Ermentrout, B. (1996). Type I membranes, phase resetting curves, and synchrony. *Neural Comput.*, *8*, 979 – 1001.

Fisahn, A., Pike, F. G., Buhl, E. H., & Paulsen, O. (1998). Cholinergic induction of network oscillations at 40 Hz in the hippocampus in vitro. *Nature*, *394*, 186 – 189.

Galarreta, M., & Hestrin, S. (2001). Electrical synapses between GABA-releasing interneurons. *Nature Reviews Neuroscience*, *2*, 425 – 433.

Gammaitoni, L., Hänggi, P., Jung, P., & Marchesoni, F. (1998). Stochastic resonance. *Reviews of Modern Physics*, *70*, 223 – 287.

Gray, C. M., & Singer, W. (1989). Stimulus-specific neuronal oscillations in orientation columns of cat visual cortex. *Proc. Natl. Acad. Sci. USA*, *86*, 1698 – 1702.

Green, P. J. (1995). Reversible jump Markov chain Monte Carlo computation and Bayesian model determination. *Biometrika*, *82*, 711 – 732.

Hegger, R., Kantz, H., & Schreiber, T. (1999). Practical implementation of nonlinear time series methods: The TISEAN package. *Chaos*, *9*, 413 – 435.

Hessler, N. A., Shirke, A. M., & Malinow, R. (1993). The probability of transmitter release at a mammalian central synapse. *Nature*, *366*, 569 – 572.

Izhikevich, E. M. (1999). Class 1 neural excitability, conventional synapses, weakly connected networks, and mathematical foundations of pulse-coupled models. *IEEE Trans. Neural Networks*, *10*, 499 – 507.

Izhikevich, E. M. (2000). Neural excitability, spiking and bursting. *Int. J. Bifurcation and Chaos*, *10*, 1171 – 1266.

Kanamaru, T. (2006). Blowout bifurcation and on-off intermittency in pulse neural networks with multiple modules. *International Journal of Bifurcation and Chaos*, *16*, 3309 – 3321.

Kanamaru, T., & Aihara, K. (2008). Stochastic synchrony of chaos in a pulse coupled neural network with both chemical and electrical synapses among inhibitory neurons. *Neural Comput.*, *20*, 1951 – 1972.

Kanamaru, T., & Aihara, K. (2012). Rewiring-induced chaos in pulse-coupled neural networks. *Neural Comput.*, *24*, 1020 – 1046.

Kanamaru, T., & Sekine, M. (2004). An analysis of globally connected active rotators with excitatory and inhibitory connections having different time constants using the nonlinear Fokker-Planck equations. *IEEE Transactions on Neural Networks*, *15*, 1009 – 1017.

Kanamaru, T., & Sekine, M. (2005). Detecting chaotic structures in noisy pulse trains based on interspike interval reconstruction. *Biological Cybernetics*, *92*, 333 – 338.

Kanamaru, T., & Sekine, M. (2006). Analysis of synchronization between two modules of pulse neural networks with excitatory and inhibitory connections. *Neural Comput.*, *18*, 1111 – 1131.

Kass, R. E., Ventura, V., & Brown, E. N. (2005). Statistical issues in the analysis of neuronal data. *J Neurophysiol.*, *94*, 8 – 25.

Kuramoto, Y. (1984). *Chemical oscillations, waves, and turbulence.* Berlin: Springer.

Lang, E. J., Sugihara, I., & Llinás, R. (1996). GABAergic modulation of complex spike activity by the cerebellar nucleoolivary pathway in rat. *Journal of Neurophysiology*, *76*, 255 – 275.

London, M., Roth, A., Beeren, L., Häusser, M., & Latham, P. E. (2010). Sensitivity to perturbations *in vivo* implies high noise and suggests rate coding in cortex. *Nature*, *466*, 123 – 127.

Monteforte, M., & Wolf, F. (2012). Dynamic flux tubes form reservoirs of stability in neuronal circuits. *Physical Review X*, *2*, 041007.

Munro, E., & Börgers, C. (2010). Mechanisms of very fast oscillations in networks of axons coupled by gap junctions. *Journal of Computational Neuroscience*, *28*, 539 – 555.

Ott, E. (2002). *Chaos in Dynamical Systems.* (2nd ed.). New York: Cambridge University Press.

Politi, A., & Torcini, A. (2010). Stable chaos. *Nonlinear dynamics and chaos: advances and perspectives*. Springer.

Ramezan, R., Marriott, P., & Chenouri, S. (2014). Multiscale analysis of neural spike trains. *Statistics in Medicine*, *33*, 238 – 256.

Sauer, T. (1994). Reconstruction of dynamical systems from interspike interval. *Rhys. Rev. Lett*, *72*, 3811 – 3814.

Schreiber, T., & Schmitz, A. (2000). Surrogate time series. *Physica D*, *142*, 346 – 382.

Shadlen, M. N., & Newsome, W. T. (1994). Noise, neural codes and cortical organization. *Current Opinion in Neurobiology*, *4*, 569 – 579.

Shimazaki, H., & Shinomoto, S. (2007). A method for selecting the bin size of a time histogram. *Neural Comput.*, *19*, 1503 – 1527.

Softky, W. R., & Koch, C. (1993). The highly irregular firing of cortical cells is inconsistent with temporal integration of random EPSPs *The Journal of Neuroscience*, *13*, 334 – 350.

Theiler. J., Eubank. S., Longtin. A., Galdrikian. B., & Farmer. J. D. (1992). Testing for nonlinearity in time series: the method for surrogate data. *Physica D*, *58*, 77 – 94.

Tiesinga, P. H. E., & José, J. V. (2000). Robust gamma oscillations in networks of inhibitory hippocampal interneurons. *Network*, *11*, 1 – 23.

Traub, R. D., Miles, R., & Wong, K. S. (1989). Model of the origin of rhythmic population oscillations in the hippocampal slice. *Science*, *243*, 1319 – 1325.

van Vreeswijk C., &Sompolinsky, H. (1996). Chaos in neuronal networks with balanced excitatory and inhibitory activity. *Science*, *274*, 1724 – 1726.

Wallstrom, G., Liebner, J., & Kass, R. E. (2008). An implementation of Bayesian adaptive regression splines (BARS) in C with S and R wrappers. *Journal of Statistical Software*, *26*, 1 – 21.

Whittington, M. A., Traub, R. D., Kopell. N., Ermentrout, B., & Buhl, E. H. (2000). Inhibition-based rhythms: experimental and mathematical observations on network dynamics. *International Journal of Psychophysiology*, *38*, 315 – 336.